Vol 17 No 10, October 2008
1674-1056/2008/17(10)/3696-08

Chinese Physics B

© 2008 Chin. Phys. Soc.
and IOP Publishing Ltd

Solution of scattering from rough surface with a 2D target above it by a hybrid method based on the reciprocity theorem and the forward–backward method*

Wang Yun-Hua(王运华)[a)†], Zhang Yan-Min(张彦敏)[b)],
He Ming-Xia(贺明霞)[b)], and Guo Li-Xin(郭立新)[c)]

[a)] *Ocean Remote Sensing Institute, Ocean University of China, Qingdao* 266003, *China*
[b)] *Department of Physics, Ocean University of China, Qingdao* 266100, *China*
[c)] *School of Science, Xidian University, Xi'an* 710071, *China*

(Received 23 November 2007; revised manuscript received 10 March 2008)

This paper proposes a hybrid method based on the forward–backward method (FBM) and the reciprocity theorem (RT) for evaluating the scattering field from dielectric rough surface with a 2D target above it. Here, the equivalent electric/magnetic current densities on the rough surface as well as the scattering field from it are numerically calculated by FBM, and the scattered field from the isolated target is obtained utilizing the method of moments (MOM). Meanwhile, the rescattered coupling interactions between the target and the surface are evaluated employing the combination of FBM and RT. Our hybrid method is first validated by available MOM results. Then, the functional dependences of bistatic and monostatic scattering from the target above rough surface upon the target altitude, incident and scattering angles are numerically simulated and discussed. This study presents a numerical description for the scattering mechanism associated with rescattered coupling interactions between a target and an underlying randomly rough surface.

Keywords: forward–backward method, reciprocity theorem, 2D target, rough surface, scattering
PACC: 4110H, 4120

1. Introduction

In recent years, there has been a great interest in studying electromagnetic scattering from a target situated above a rough surface.[1−7] It is well known that the theoretical and numerical approaches associated with targets in the vicinity of a planar interface have been studied extensively by many researchers.[8−16] However, considering the interface to be a rough surface is a new challenge. Ye *et al* proposed an iterative approach to differentiate scattering field from a 2D target above a 2D rough surface.[1] In Ref.[1], it should be pointed out that both the target and the rough surface are perfectly electric conducting (PEC). In Refs.[2, 3], the four-path model has been used to evaluate the scattering field from an object above a planar or rough surface. Nevertheless, as discussed in Section 4 of this paper, the results obtained via the four-path model are not always accurate. In Ref.[5], the electromagnetic scattering from a PEC target located above or below rough surface is investigated, for the case of TM polarization, using the method of moments (MOM). Based on reciprocity theorem (RT), a solution for the rescattered fields between a dielectric cylinder and a slightly rough surface is presented by Chiu *et al*.[6] However, in Ref.[6], the coupling interactions between the target and the surface are represented to be the double bounce model.

The forward–backward method (FBM) has been shown to be an extremely efficient iterative MOM for the computation of scattering field from 2D dielectric rough surface.[17] On the other hand, as already discussed in Refs.[6, 18–20], RT can be used to treat with the problems of electromagnetic scattering from two adjacent targets. The objective of this paper is to present a hybrid RT/FBM method for evaluating the electromagnetic scattering from a 2D target above a 2D randomly rough surface. Here, dielectric materials are considered for the target and the underlying rough surface. In our work, the equivalent electric/magnetic current densities on the rough surface as well as the scattering fields from it are numerically calculated by

*Project supported by the National Natural Science Foundation of China (Grant No 60571058) and the National Defense Foundation of China.
†E-mail: wyh78917@yahoo.com.cn

FBM, and the scattered field from the isolated target is obtained utilizing the MOM. Meanwhile, the rescattered coupling fields between the target and the underlying surface are evaluated employing the combination of FBM and RT. Here, a compromise approach to model the target-surface problem assumes that the scattered waves consist of rays which are reflected off the surface either before or after interacting with the target.

This paper is organized as follows. The equivalent model of the scattering problem is presented in the next Section. In Section 3, the main concepts of FBM are briefly reviewed and the composite scattering field is evaluated by the RT/FBM method. In Sections 4 and 5, the numerical results and the conclusions are reported, respectively.

2. Scattering model

Figure 1 illustrates the basic geometry considered in this paper: a dielectric 2D target is situated above a dielectric randomly rough interface $y = f(x)$ with a plane incident wave propagating toward the rough interface. Assume that the scattered field consists of rays that are reflected off the randomly rough surface either before or after interacting with the target, as shown in Fig.2(a–i), the composite scattering field would be the superposition of the directly scattered field $\boldsymbol{E}_1^{\mathrm{s}}$ and $\boldsymbol{E}_2^{\mathrm{s}}$, as well as the rescattered fields $\boldsymbol{E}_3^{\mathrm{s}}$, $\boldsymbol{E}_4^{\mathrm{s}}$, $\boldsymbol{E}_5^{\mathrm{s}}$, $\boldsymbol{E}_6^{\mathrm{s}}$, $\boldsymbol{E}_7^{\mathrm{s}}$, $\boldsymbol{E}_8^{\mathrm{s}}$ and $\boldsymbol{E}_9^{\mathrm{s}}$, i.e.

$$\boldsymbol{E}^{\mathrm{s}} = \boldsymbol{E}_1^{\mathrm{s}} + \boldsymbol{E}_2^{\mathrm{s}} + \boldsymbol{E}_3^{\mathrm{s}} + \boldsymbol{E}_4^{\mathrm{s}} + \boldsymbol{E}_5^{\mathrm{s}} + \boldsymbol{E}_6^{\mathrm{s}} + \boldsymbol{E}_7^{\mathrm{s}} + \boldsymbol{E}_8^{\mathrm{s}} + \boldsymbol{E}_9^{\mathrm{s}}. \quad (1)$$

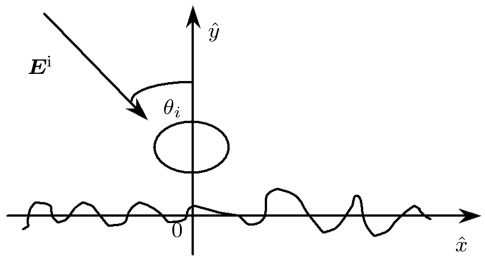


Fig.1. Geometry of the problem.

In the case that the underlying dielectric rough surface is replaced by a planar interface, the corresponding scattering models, which are equivalent to the models shown in Fig.2(a–i), are illustrated in Fig.3(a-i) utilizing the image theory. As shown in Fig.3, the third- and the higher-order rescattered fields between actual scatterer and the image one have been neglected, and the validity of this approximation has been discussed in Refs.[19, 20].

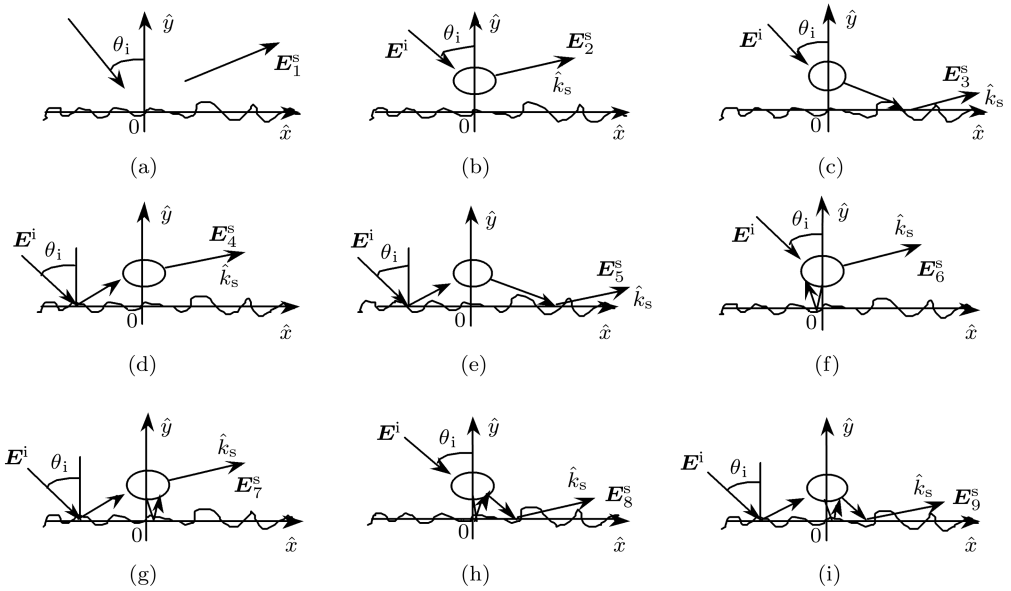


Fig.2. Scattering mechanism of the problem.

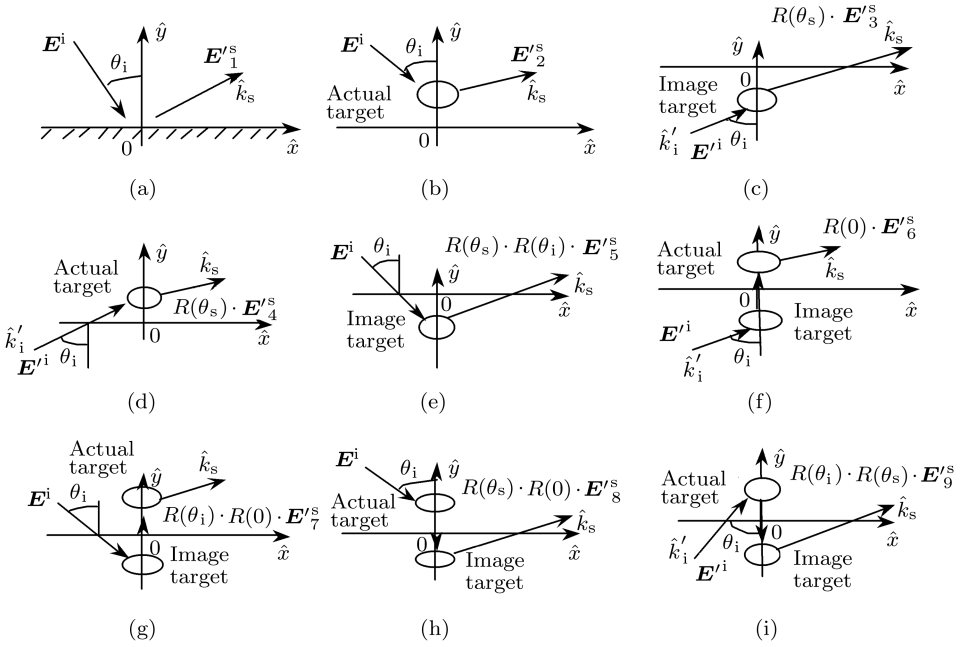


Fig.3. The corresponding equivalent scattering models of Fig.2 while the underlying interface is planar.

In Ref.[6], the coupling interactions between the target and the slightly rough surface are represented by the double bounce model, which suggests that the composite scattered fields are likely to be dominated by paths that involve $\boldsymbol{E}_1^{\mathrm{s}}$,$\boldsymbol{E}_2^{\mathrm{s}}$, $\boldsymbol{E}_3^{\mathrm{s}}$ and $\boldsymbol{E}_4^{\mathrm{s}}$. And in Refs.[2,3], the scattering problem of the present work has been solved by four-path model, which suggests that the composite scattered fields are likely to be dominated by paths which involve $\boldsymbol{E}_1^{\mathrm{s}}$,$\boldsymbol{E}_2^{\mathrm{s}}$, $\boldsymbol{E}_3^{\mathrm{s}}$, $\boldsymbol{E}_4^{\mathrm{s}}$ and $\boldsymbol{E}_5^{\mathrm{s}}$. However, when underlying interface is planar, from Fig.3, it is obvious that the second-order coupling fields between the actual target and the image one have been neglected both in the double bounce model and the four-path model. Whereas, as discussed in Section 4, the results obtained by four-path model are not always acceptable.

3. Calculation of the composite scattering field

3.1. The iterative forward–backward method

In Ref.[17], it has been shown that the iterative FBM is an efficient method for numerical evaluation of scattering from dielectric rough surface. Here, this numerical method also has been used to calculate the scattering field from the underlying rough surface. So, it is necessary to recall firstly the main concepts of this method. If the incident field is TE (horizontally polarized) polarization, the surface electric and magnetic fields can be evaluated by solving the following pair of integral scalar equations:[21]

$$\begin{aligned}\boldsymbol{E}^{\mathrm{i}}(\boldsymbol{\rho}) &= \frac{1}{2}\boldsymbol{E}(\boldsymbol{\rho}) + \int_l \{\mathrm{i}\omega\mu_0\phi_0(\boldsymbol{\rho},\boldsymbol{\rho}')\boldsymbol{J}_{\mathrm{s}}(\boldsymbol{\rho}') \\ &\quad + \boldsymbol{E}(\boldsymbol{\rho}')[\hat{\boldsymbol{n}}'\cdot\nabla\phi_0(\boldsymbol{\rho},\boldsymbol{\rho}')]\}\mathrm{d}l', \qquad (2)\\ 0 &= \frac{1}{2}\boldsymbol{E}(\boldsymbol{\rho}) - \int_l \{\mathrm{i}\omega\mu_0\phi_1(\boldsymbol{\rho},\boldsymbol{\rho}')\boldsymbol{J}_{\mathrm{s}}(\boldsymbol{\rho}') \\ &\quad + \boldsymbol{E}(\boldsymbol{\rho}')[\hat{\boldsymbol{n}}'\cdot\nabla\phi_1(\boldsymbol{\rho},\boldsymbol{\rho}')]\}\mathrm{d}l', \qquad (3)\end{aligned}$$

where $\boldsymbol{E}^{\mathrm{i}} = E^{\mathrm{i}}\hat{\boldsymbol{y}}$ and $\boldsymbol{E} = E\hat{\boldsymbol{y}}$ are the incident and total electric field, respectively. $\boldsymbol{J}_{\mathrm{s}} = \hat{\boldsymbol{n}}\times\boldsymbol{H} = J_{\mathrm{s}}\hat{\boldsymbol{y}}$ is the equivalent surface electric current density, $\hat{\boldsymbol{n}}$ is the outgoing normal to the surface.

$$\phi_{0,1}(\boldsymbol{\rho},\boldsymbol{\rho}') = -\frac{\mathrm{i}}{4}H_0^{(2)}(k_{0,1}|\boldsymbol{\rho}-\boldsymbol{\rho}'|). \qquad (4)$$

where $\phi_{0,1}(\boldsymbol{\rho},\boldsymbol{\rho}')$ is the Green's function in the 2-D space, k_0 and k_1 are the propagation constants of free-space and the target, respectively. $H_0^{(2)}(\cdot)$ is the zero order Hankel function of the second kind, and l denotes the profile of the target. $\boldsymbol{\rho}$ and $\boldsymbol{\rho}'$ both belong to the target's profile. Equations (2) and (3) are obtained as a simple application of the equivalence theorem.

Using rectangular pulse basis functions and the point matching method, we can convert Eqs.(2) and

(3) into the following matrix equation in the unknowns $\boldsymbol{E}$ and $\boldsymbol{J}_{\rm s}$:

$$\begin{aligned}\boldsymbol{S}_0\boldsymbol{E}+\boldsymbol{Z}_0\boldsymbol{J}_{\rm s}&=\boldsymbol{E}^{\rm i},\\ \boldsymbol{S}_1\boldsymbol{E}+\boldsymbol{Z}_1\boldsymbol{J}_{\rm s}&=0.\end{aligned}\tag{5}$$

Equation (5) can be expressed in a more compact form as $\boldsymbol{A}\cdot\boldsymbol{x}=\boldsymbol{y}$. Here, the size of the matrix $\boldsymbol{A}$ is $2N\times 2N$, N is the number of rectangular pulse basis functions used to expand the unknown functions. Start from Eq.(5) and let

$$\begin{aligned}\boldsymbol{E}&=\boldsymbol{E}^{\rm f}+\boldsymbol{E}^{\rm b},\\ \boldsymbol{J}_{\rm s}&=\boldsymbol{J}_{\rm s}^{\rm f}+\boldsymbol{J}_{\rm s}^{\rm b},\end{aligned}\tag{6}$$

and

$$\begin{aligned}\boldsymbol{S}_0&=\boldsymbol{S}_0^{\rm L}+\boldsymbol{S}_0^{\rm D}+\boldsymbol{S}_0^{\rm U},\\ \boldsymbol{Z}_0&=\boldsymbol{Z}_0^{\rm L}+\boldsymbol{Z}_0^{\rm D}+\boldsymbol{Z}_0^{\rm U},\\ \boldsymbol{S}_1&=\boldsymbol{S}_1^{\rm L}+\boldsymbol{S}_1^{\rm D}+\boldsymbol{S}_1^{\rm U},\\ \boldsymbol{Z}_1&=\boldsymbol{Z}_1^{\rm L}+\boldsymbol{Z}_1^{\rm D}+\boldsymbol{Z}_1^{\rm U},\end{aligned}\tag{7}$$

where $\boldsymbol{E}^{\rm f}$ and $\boldsymbol{J}_{\rm s}^{\rm f}$ are the forward components of magnetic and electric equivalent surface sources, respectively, $\boldsymbol{E}^{\rm b}$ and $\boldsymbol{J}_{\rm s}^{\rm b}$ are the backward components. In addition, $\boldsymbol{S}_{0,1}^{\rm L}$ and $\boldsymbol{Z}_{0,1}^{\rm L}$ are the lower triangular part of $\boldsymbol{S}_{0,1}$ and $\boldsymbol{Z}_{0,1}$; $\boldsymbol{S}_{0,1}^{\rm D}$ and $\boldsymbol{Z}_{0,1}^{\rm D}$ are the diagonal part; $\boldsymbol{S}_{0,1}^{\rm U}$ and $\boldsymbol{Z}_{0,1}^{\rm U}$ are the upper triangular part. Then, Eq.(5) can be decomposed into forward- and backward- propagation pairs of equations

$$\begin{aligned}&\boldsymbol{S}_0^{\rm D}\boldsymbol{E}^{\rm f}+\boldsymbol{Z}_0^{\rm D}\boldsymbol{J}_{\rm s}^{\rm f}\\ =\;&\boldsymbol{E}^{\rm i}-\boldsymbol{S}_0^{\rm L}(\boldsymbol{E}^{\rm f}+\boldsymbol{E}^{\rm b})-\boldsymbol{Z}_0^{\rm L}(\boldsymbol{J}_{\rm s}^{\rm f}+\boldsymbol{J}_{\rm s}^{\rm b}),\\ &\boldsymbol{S}_1^{\rm D}\boldsymbol{E}^{\rm f}+\boldsymbol{Z}_1^{\rm D}\boldsymbol{J}_{\rm s}^{\rm f}\\ =\;&-\boldsymbol{S}_1^{\rm L}(\boldsymbol{E}^{\rm f}+\boldsymbol{E}^{\rm b})-\boldsymbol{Z}_1^{\rm L}(\boldsymbol{J}_{\rm s}^{\rm f}+\boldsymbol{J}_{\rm s}^{\rm b}),\end{aligned}\tag{8}$$

$$\begin{aligned}&\boldsymbol{S}_0^{\rm D}\boldsymbol{E}^{\rm b}+\boldsymbol{Z}_0^{\rm D}\boldsymbol{J}_{\rm s}^{\rm b}\\ =\;&-\boldsymbol{S}_0^{\rm U}(\boldsymbol{E}^{\rm f}+\boldsymbol{E}^{\rm b})-\boldsymbol{Z}_0^{\rm U}(\boldsymbol{J}_{\rm s}^{\rm f}+\boldsymbol{J}_{\rm s}^{\rm b}),\\ &\boldsymbol{S}_1^{\rm D}\boldsymbol{E}^{\rm b}+\boldsymbol{Z}_1^{\rm D}\boldsymbol{J}_{\rm s}^{\rm b}\\ =\;&-\boldsymbol{S}_1^{\rm U}(\boldsymbol{E}^{\rm f}+\boldsymbol{E}^{\rm b})-\boldsymbol{Z}_1^{\rm U}(\boldsymbol{J}_{\rm s}^{\rm f}+\boldsymbol{J}_{\rm s}^{\rm b}).\end{aligned}\tag{9}$$

Equations (8) and (9) can be calculated by iterative technique, and the detailed procedure has been discussed in Ref.[17].

After the unknowns $\boldsymbol{E}$ and $\boldsymbol{J}_{\rm s}$ have been obtained by solving the matrix equations (8) and (9), then, the equivalent surface magnetic current density on the rough surface and the scattered field in the free space can be evaluated by the following equations

$$\boldsymbol{M}_{\rm s}=-\hat{\boldsymbol{n}}\times\boldsymbol{E},\tag{10}$$

$$\begin{aligned}\boldsymbol{E}^{\rm s}(\boldsymbol{\rho})=\;&\frac{k_0}{4}\int_l\{Z_0\boldsymbol{J}_{\rm s}(\boldsymbol{\rho}')-\boldsymbol{E}(\boldsymbol{\rho}')[\hat{\boldsymbol{n}}'\cdot\hat{\boldsymbol{k}}_{\rm s}]\}\\ &\times H_0^2(k_{\rm s}|\boldsymbol{\rho}-\boldsymbol{\rho}'|){\rm d}l',\end{aligned}\tag{11}$$

where $\hat{\boldsymbol{k}}_{\rm s}$ is the unit vector indicating the scattering direction, Z_0 is the free-space intrinsic impedance.

For the case of TM (vertically polarized) polarization, similar procedure can be applied.

3.2. Composite scattered field

In Eq.(1), $\boldsymbol{E}_1^{\rm s}$ and $\boldsymbol{E}_2^{\rm s}$ can be evaluated by FBM and MOM directly. However, the other seven scattered terms, i.e. $\boldsymbol{E}_3^{\rm s}$, $\boldsymbol{E}_4^{\rm s}$, $\boldsymbol{E}_5^{\rm s}$, $\boldsymbol{E}_6^{\rm s}$, $\boldsymbol{E}_7^{\rm s}$, $\boldsymbol{E}_8^{\rm s}$ and $\boldsymbol{E}_9^{\rm s}$, denote the rescattered fields between the target and the underlying rough surface. To obtain the solutions of these seven terms, unfortunately, it is necessary to treat electromagnetic interaction, which is not only non-plane-wave in character but have non-uniformities in amplitude and phase, between the target and the rough surface. For this type of problem, the exact analytical solutions cannot be found. To overcome these difficulties, a hybrid method is proposed to calculate the interaction fields employing the FBM and RT. In the following discussion, the hybrid method is presented.

Let an incident plane wave of unit amplitude illuminates on the target and the underlying surface. The formula for the incident wave can be written as

$$\boldsymbol{E}^{\rm i}=\hat{\boldsymbol{q}}\exp({\rm i}\boldsymbol{k}_{\rm i}\cdot\boldsymbol{\rho}),\tag{12}$$

where $\hat{\boldsymbol{q}}$ denotes $\hat{\boldsymbol{v}}_{\rm i}$ (TM) or $\hat{\boldsymbol{h}}_{\rm i}$ (TE), $\hat{\boldsymbol{q}}$ and $\boldsymbol{k}_{\rm i}$ are the unit polarization vector and wave-number vector of the incident wave, respectively.

Suppose a line electric current source $\boldsymbol{J}_{\rm e}=\hat{\boldsymbol{p}}\delta(\boldsymbol{\rho}-\boldsymbol{\rho}_0)$ and a line magnetic current source $\boldsymbol{M}_m=\hat{\boldsymbol{q}}\delta(\boldsymbol{\rho}-\boldsymbol{\rho}_0)$ are placed at the far-zone observation point. Here, the unit polarization vector $\hat{\boldsymbol{q}}$ ($\hat{\boldsymbol{v}}_{\rm s}$ or $\hat{\boldsymbol{h}}_{\rm s}$) and $\hat{\boldsymbol{p}}$ ($\hat{\boldsymbol{v}}_{\rm s}$ or $\hat{\boldsymbol{h}}_{\rm s}$) are related by $\hat{\boldsymbol{q}}=\hat{\boldsymbol{k}}_{\rm s}\times\hat{\boldsymbol{p}}$, $\boldsymbol{\rho}_0$ is the position vector of the far-zone observation point. Along the wave-number vector $\hat{\boldsymbol{k}}_{\rm s}$, the direct electric field generated by $\boldsymbol{J}_{\rm e}$ and the direct magnetic field generated by $\boldsymbol{M}_{\rm m}$ can be written as[19,20]

$$\begin{aligned}\boldsymbol{E}_{\rm ed}(\boldsymbol{\rho})=\;&\frac{-k_0Z_0}{2\sqrt{2\pi k_0\rho_0}}\exp\left({\rm i}k_0\rho_0-{\rm i}\frac{\pi}{4}\right)\\ &\times\exp(-{\rm i}\boldsymbol{k}_{\rm s}\cdot\boldsymbol{\rho})\hat{\boldsymbol{k}}_{\rm s}\times\hat{\boldsymbol{k}}_{\rm s}\times\hat{\boldsymbol{p}},\end{aligned}\tag{13}$$

and

$$\begin{aligned}\boldsymbol{H}_{\rm md}(\boldsymbol{\rho})=\;&\frac{-k_0Y_0}{2\sqrt{2\pi k_0\rho_0}}\exp\left({\rm i}k_0\rho_0-{\rm i}\frac{\pi}{4}\right)\\ &\times\exp(-{\rm i}\boldsymbol{k}_{\rm s}\cdot\boldsymbol{\rho})\hat{\boldsymbol{k}}_{\rm s}\times\hat{\boldsymbol{k}}_{\rm s}\times\hat{\boldsymbol{q}}.\end{aligned}\tag{14}$$

When the underlying surface is illuminated by $\boldsymbol{E}_{\rm ed}$ and $\boldsymbol{H}_{\rm md}$, the corresponding scattered fields $\boldsymbol{E}_{\rm edr}$ and $\boldsymbol{H}_{\rm mdr}$ can be calculated by FBM. Meanwhile, the equivalent surface electric current density $\boldsymbol{J}_{\rm t}$ and the equivalent surface magnetic current density $\boldsymbol{M}_{\rm t}$ on the target's surface, which are induced by the incident field $\boldsymbol{E}^{\rm i}$, can be evaluated by MOM.

Then, based on RT,[19,20] we get

$$\begin{aligned}\hat{\boldsymbol{p}}\cdot\boldsymbol{E}'^{\rm s}_{\rm J3}&=\int_{l_{\rm t}}\boldsymbol{E}_{\rm edr}\cdot\boldsymbol{J}_{\rm t}{\rm d}l,\\ \hat{\boldsymbol{q}}\cdot\boldsymbol{H}'^{\rm s}_{\rm M3}&=\int_{l_{\rm t}}\boldsymbol{H}_{\rm mdr}\cdot\boldsymbol{M}_{\rm t}{\rm d}l.\end{aligned}\tag{15}$$

where $l_{\rm t}$ represents the profile of the target's surface. Similarly, it is obtained that

$$\begin{aligned}\hat{\boldsymbol{p}}\cdot\boldsymbol{E}'^{\rm s}_{\rm J4}&=\int_{l_{\rm r}}\boldsymbol{E}_{\rm edt}\cdot\boldsymbol{J}_{\rm r}{\rm d}l,\\ \hat{\boldsymbol{q}}\cdot\boldsymbol{H}'^{\rm s}_{\rm M4}&=\int_{l_{\rm r}}\boldsymbol{H}_{\rm edt}\cdot\boldsymbol{M}_{\rm r}{\rm d}l,\end{aligned}\tag{16}$$

where $l_{\rm r}$ represents the profile of the underlying surface, $\mathbf{E}_{\rm edt}$ and $\boldsymbol{H}_{\rm edt}$ are the scattered field when the target is illuminated by $\boldsymbol{E}_{\rm ed}$ and $\boldsymbol{H}_{\rm md}$, respectively. $\boldsymbol{J}_{\rm r}$ and $\boldsymbol{M}_{\rm r}$ are the equivalent surface current density induced by $\boldsymbol{E}^{\rm i}$.

Taking the scattered field of $\boldsymbol{E}^{\rm i}$ from underlying surface as the incident field to illuminate the 2D target, we can evaluate the equivalent surface electric density $\boldsymbol{J}_{\rm rt}$ and the equivalent surface magnetic current density $\boldsymbol{M}_{\rm rt}$ on the profile of the target by MOM. Then, based on RT, we can obtain

$$\begin{aligned}\hat{\boldsymbol{p}}\cdot\boldsymbol{E}'^{\rm s}_{\rm J5}&=\int_{l_{\rm t}}\boldsymbol{E}_{\rm edr}\cdot\boldsymbol{J}_{\rm rt}{\rm d}l,\\ \hat{\boldsymbol{q}}\cdot\boldsymbol{H}'^{\rm s}_{\rm M5}&=\int_{l_{\rm t}}\boldsymbol{H}_{\rm mdr}\cdot\boldsymbol{M}_{\rm rt}{\rm d}l.\end{aligned}\tag{17}$$

Using the similar method, we obtain

$$\begin{aligned}\hat{\boldsymbol{p}}\cdot\boldsymbol{E}'^{\rm s}_{\rm J6}&=\int_{l_{\rm r}}\boldsymbol{E}_{\rm edt}\cdot\boldsymbol{J}_{\rm tr}{\rm d}l,\\ \hat{\boldsymbol{q}}\cdot\boldsymbol{H}'^{\rm s}_{\rm M6}&=\int_{l_{\rm r}}\boldsymbol{H}_{\rm mdt}\cdot\boldsymbol{M}_{\rm tr}{\rm d}l,\end{aligned}\tag{18}$$

$$\begin{aligned}\hat{\boldsymbol{p}}\cdot\boldsymbol{E}'^{\rm s}_{\rm J7}&=\int_{l_{\rm r}}\boldsymbol{E}_{\rm edt}\cdot\boldsymbol{J}_{\rm rtr}{\rm d}l,\\ \hat{\boldsymbol{q}}\cdot\boldsymbol{H}'^{\rm s}_{\rm M7}&=\int_{l_{\rm r}}\boldsymbol{H}_{\rm mdt}\cdot\boldsymbol{M}_{\rm rtr}{\rm d}l,\end{aligned}\tag{19}$$

$$\begin{aligned}\hat{\boldsymbol{p}}\cdot\boldsymbol{E}'^{\rm s}_{\rm J8}&=\int_{l_{\rm t}}\boldsymbol{E}_{\rm edr}\cdot\boldsymbol{J}_{\rm trt}{\rm d}l,\\ \hat{\boldsymbol{q}}\cdot\boldsymbol{H}'^{\rm s}_{\rm M8}&=\int_{l_{\rm t}}\boldsymbol{H}_{\rm mdr}\cdot\boldsymbol{M}_{\rm trt}{\rm d}l,\end{aligned}\tag{20}$$

and

$$\begin{aligned}\hat{\boldsymbol{p}}\cdot\boldsymbol{E}'^{\rm s}_{\rm J9}&=\int_{l_{\rm t}}\boldsymbol{E}_{\rm edr}\cdot\boldsymbol{J}_{\rm rtrt}{\rm d}l,\\ \hat{\boldsymbol{q}}\cdot\boldsymbol{H}'^{\rm s}_{\rm M9}&=\int_{l_{\rm t}}\boldsymbol{H}_{\rm mdr}\cdot\boldsymbol{M}_{\rm rtrt}{\rm d}l.\end{aligned}\tag{21}$$

In Eqs.(18–21), the last character r (rough surface) and t (target) of the subscripts of the current density denote that the current density is on the profile of rough surface and on the profile of the target, respectively. The other characters of the subscripts of the current density denote the scattering path of the reaction field, such as $\boldsymbol{J}_{\rm trt}$ expresses the surface electric current density on the profile of the target when it is illuminated by the rescattered field from the underlying surface of the scattered field from the target.

Using Eqs.(15–21), we obtain the composite scattering field

$$\begin{aligned}\hat{\boldsymbol{p}}\cdot\boldsymbol{E}^{\rm s}&=\hat{\boldsymbol{p}}\cdot(\boldsymbol{E}^{\rm s}_1+\boldsymbol{E}^{\rm s}_2+\boldsymbol{E}^{\rm s}_3+\boldsymbol{E}^{\rm s}_4+\boldsymbol{E}^{\rm s}_5+\boldsymbol{E}^{\rm s}_6\\&\quad+\boldsymbol{E}^{\rm s}_7+\mathbf{E}^{\rm s}_8+\boldsymbol{E}^{\rm s}_9)\\&=\hat{\boldsymbol{p}}\cdot[\boldsymbol{E}^{\rm s}_1+\boldsymbol{E}^{\rm s}_2+(\boldsymbol{E}'^{\rm s}_{\rm J3}+\boldsymbol{E}'^{\rm s}_{\rm M3})\\&\quad+(\boldsymbol{E}'^{\rm s}_{\rm J4}+\boldsymbol{E}'^{\rm s}_{\rm M4})+(\boldsymbol{E}'^{\rm s}_{\rm J5}+\mathbf{E}'^{\rm s}_{\rm M5})\\&\quad+(\boldsymbol{E}'^{\rm s}_{\rm J6}+\boldsymbol{E}'^{\rm s}_{\rm M6})+(\mathbf{E}'^{\rm s}_{\rm J7}+\boldsymbol{E}'^{\rm s}_{\rm M7})\\&\quad+(\boldsymbol{E}'^{\rm s}_{\rm J8}+\boldsymbol{E}'^{\rm s}_{\rm M8})+(\boldsymbol{E}'^{\rm s}_{\rm J9}+\boldsymbol{E}'^{\rm s}_{\rm M9})].\end{aligned}\tag{22}$$

In Eq.(22), the relation $\boldsymbol{E}'^{\rm s}_{\rm M}=-Z_0\hat{\boldsymbol{k}}_{\rm s}\times\boldsymbol{H}'^{\rm s}_{\rm M}$ has been used.

4. Numerical results

In the following discussions, only TE (horizontally polarized) polarization case is considered due to the limited length of the article.

In Fig.4, bistatic scattering results are compared with the data obtained by MOM. Here, the length and the correlation length (col) of the underlying Gaussian rough surface are $l=12.8\lambda$ and col $=0.5\lambda$ respectively, root mean square (rms) of the surface in Figs.4(a) and 4(b) are rms $=0.01\lambda$ and rms $=0.03\lambda$ respectively. The distance between the cylindrical target axial line and the rough surface is $h=2\lambda$, the radius of the cylinder is $r=0.5\lambda$, the relative dielectric constant of the target and the rough surface equals to 20. Figure 5 gives the scattering angle patterns of the monostatic scattering width for different underlying surface. In Fig.5, the parameters of the surface and the target are the same as those in Fig.4 except that the distance between the cylindrical target axial's line and the rough surface is $h=5\lambda$, the radius of the cylinder is $r=1\lambda$, the relative dielectric constant of

the target and the rough surface is $\varepsilon_r = 2.0$. The relative errors between the results obtained by our method and the numerical computations based on MOM are also illustrated in the top sub-images of Figs.4 and 5. From Figs.4 and 5, it is obvious that the results of our approach provide more reasonable approximations than that obtained via four-path method. And as shown in the top sub-images, the relative errors of our method are less than 3dB for most scattering angles.

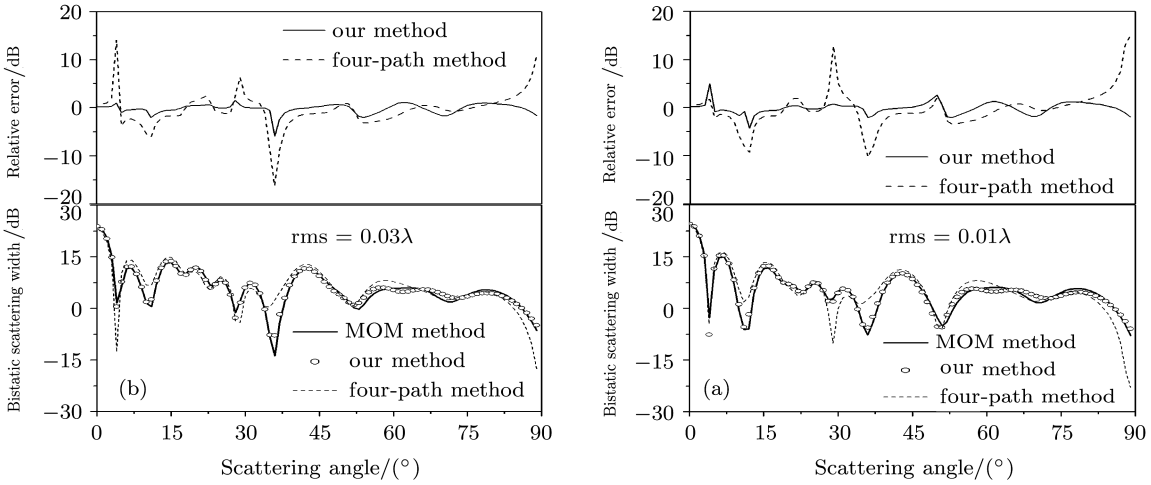


Fig.4. Bistatic scattering width of the target for different underlying surface ($\theta_i = 0°$).

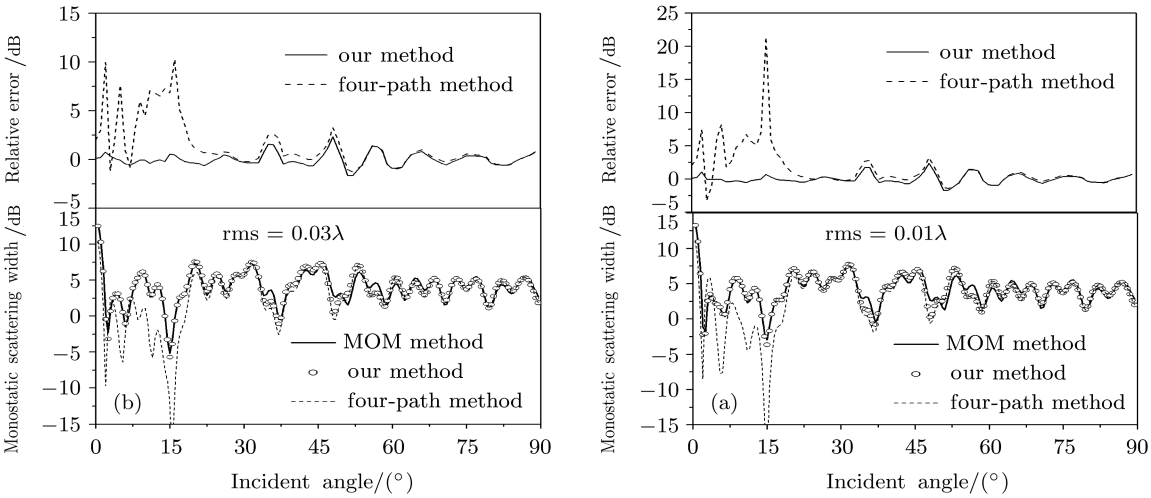


Fig.5. Monostatic scattering width of the target for different underlying surface.

Figure 6 shows bistatic scattering for different incident angles. Here, the distance between the cylindrical target's axial line and the rough surface is $h = 5\lambda$, the radius of the cylinder is $r = 1\lambda$, and the other parameters are the same as those in Fig.4. Comparing with Fig.4, we can find that the difference between the results obtained by the four-path method and by our method becomes less as the incident angle increases. The reason of this phenomenon is that the rescattered fields $\boldsymbol{E}_6^s$, $\boldsymbol{E}_7^s$, $\boldsymbol{E}_8^s$ and $\boldsymbol{E}_9^s$ will become very weak and can be neglected when the incident angle is large.

In Fig.7, the distance between the cylindrical target's axial line and the rough surface is $h = 4\lambda$, root mean square of the surface is rms $= 0.01\lambda$ and the other parameters are the same as those in Fig.4. From Figs.7 (a) and 7(b), it is found that the amplitude of the angle patterns for the composite scattering models is larger than that for the Gaussian surface. From Fig.7, one can also see that, with the decrease of r, the results of the composite model will gradually approach to those of the Gaussian surface.

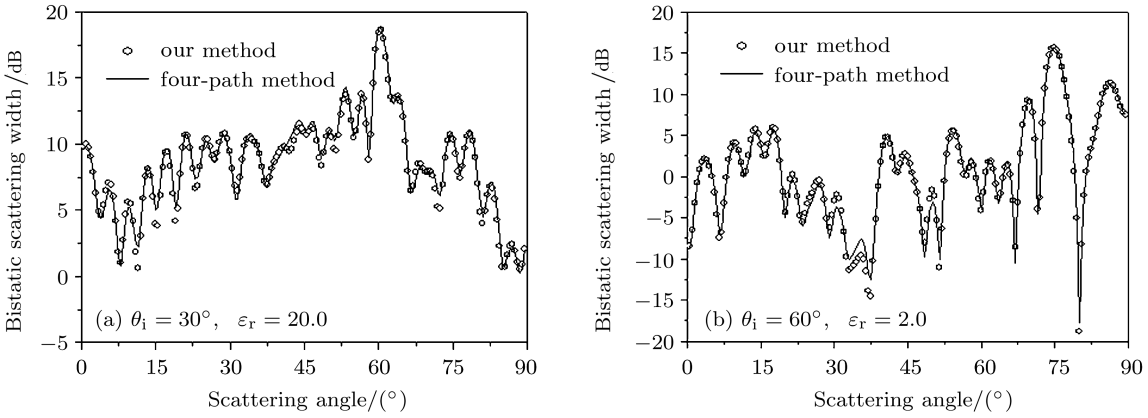


Fig.6. Bistatic scattering width of the target for different incident angles.

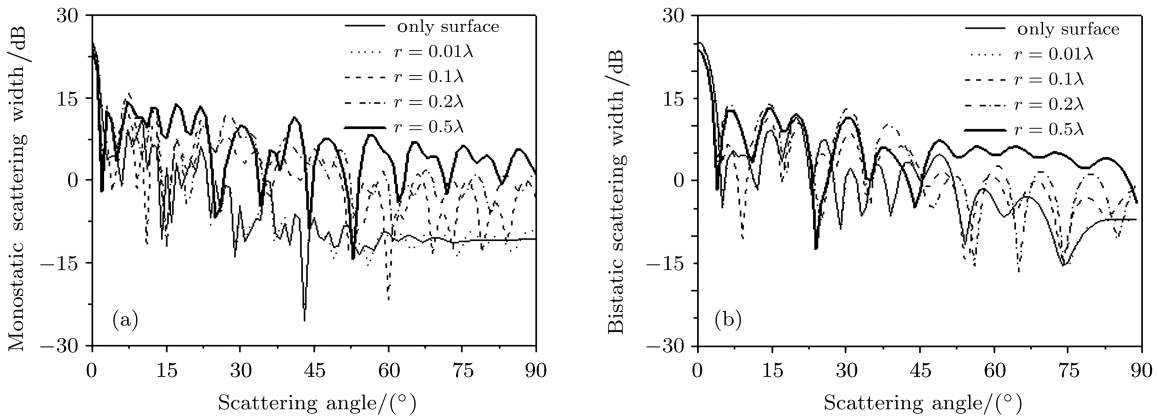


Fig.7. Scattering width from the composite scattering model for different target: (a) monostatic; (b) bistatic.

A relationship between backscattering width and h is shown in Fig.8. Here, the relative dielectric constant of the target and the rough surface equals to 2.0, rms and col of the surface are 0.05λ and 0.5λ, respectively. The other parameters are the same as those in Fig.4. From this figure, it can be seen that the value of the scattered width periodically fluctuates with increasing h. This is mainly because that the scattering fields $\boldsymbol{E}_2^s$, $\boldsymbol{E}_3^s$, $\boldsymbol{E}_4^s$ and $\boldsymbol{E}_5^s$ interfere with each other.

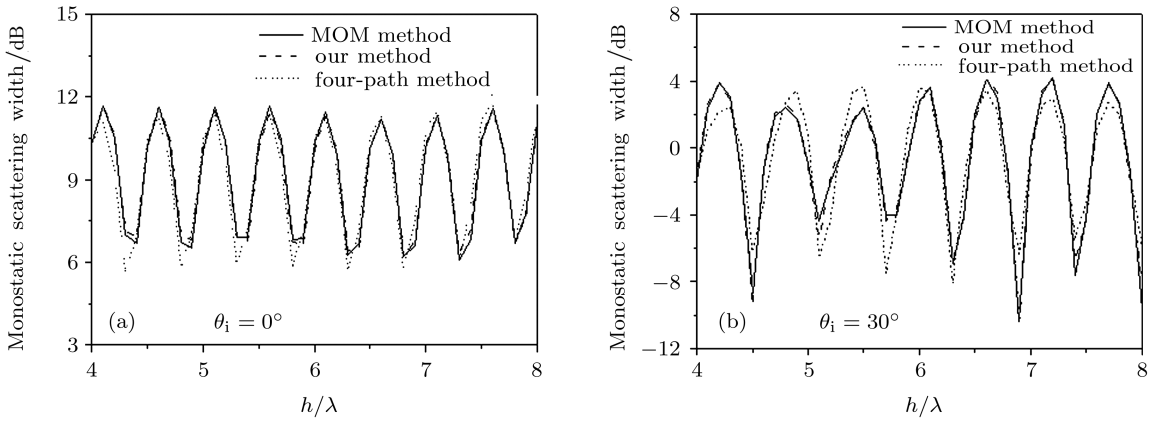


Fig.8. Monostatic scattering width versus target altitude.

5. Conclusion

Based on FBM and RT, a hybrid method is presented for evaluating the scattering field from a rough surface with a 2D dielectric target above it. The validity of this hybrid method is verified by comparing our numerical results with the data obtained by MOM. Compared with the four-path model, we find that our method is more reasonable. Furthermore, compared with analytical method, our method has two advantages: (1) complicated formulas are avoided; (2) it can be applied to evaluate the scattering field from arbitrary shaped 2D target. Finally, the functional dependences of bistatic and monostatic scattering from the target above rough surface upon the target altitude, incident and scattering angle are numerically simulated and discussed. It should be pointed out that the method proposed in this work can also be extended to the problem of the electromagnetic scattering from 3D targets.

References

[1] Ye H X and Jin Y Q 2006 *IEEE Trans. Geosci. Remote Sens.* **44** 108
[2] Johnson J T 2001 *Microwave and optical technology letters* **30** 130
[3] Johnson J T 2002 *IEEE Trans. Antennas Propagat.***50** 1361
[4] Liu P and Jin Y Q 2004 *IEEE Trans. Geosci. Remote Sens.* **52** 1205
[5] Wang X, Wang C F , Gan Y B and Li L W 2003 *Progress In Electromagnetics Research PIER* **40** 207
[6] Chiu T and Sarabandi K 1999 *IEEE Trans. Antennas Propagat.* **47** 902
[7] Wang R, Guo L X and Wang Y H 2007 *J. Xidian University* **34** 958 (in Chinese)
[8] Videen G 1991 *J. Opt. Soc. Am.* A **8** 483
[9] Johnson B R 1994 *J. Opt. Soc. Am.* A **11** 2055
[10] Videen G 1993 *J. Opt. Soc. Am.* A **10** 110
[11] Videen G 1993*J. Opt. Soc. Am.* A **10** 118
[12] Fucile E ,Denti P, Borghese F, Saija R and Sindoni O L 1997 *J. Opt. Soc. Am.* A **14** 1505
[13] Videen G and Ngo D 1997 *J. Opt. Soc. Am.* A **14** 70
[14] Borghi R, Gori F and Santarsiero M 1996 *J. Opt. Soc. Am.* A **13** 2441
[15] Valle P J, Gonzalez F and Moreno F 1994 *Appl. Opt.* **33** 512
[16] Bertrand J C and Young J W 1975*J. Opt. Soc. Am.* A **60** 1265
[17] Iodice A 2004 *IEEE Trans. Geosci. Remote Sens.* **42** 77
[18] Sarabandi K and Polatin P F 1994 *IEEE Trans. Antennas Propagat.* **42** 510
[19] Wang Y H, Guo L X and Wu Z S 2007 *Radio Science* **42** RS4012
[20] Wang Y H, Guo L X and Wu Q 2006 *Chin. Phys.* **15** 1755
[21] Franceschetti G, Iodice A and Riccio D 2000 *IEEE Trans. Antennas Propagat.* **38** 1644